Impact of quenched random fields on the ferroelectric-to-relaxor crossover in the solid solution $(1 − x)$BaTiO$_3$−xDyFeO$_3$

Jian Zhuang,[1,*] Alexei A. Bokov,[1,2,†] Nan Zhang,[1] David Walker,[3] Siqi Huo,[2] Jie Zhang,[1] Wei Ren,[1] and Zuo-Guang Ye[1,2,‡]

[1]*Electronic Materials Research Laboratory, Key Laboratory of the Ministry of Education and International Centre for Dielectric Research, School of Electronic and Information Engineering, Xi'an Jiaotong University, Xi'an 710049, China*

[2]*Department of Chemistry and 4D LABS, Simon Fraser University, Burnaby, British Columbia, Canada V5A 1S6*

[3]*Department of Physics, University of Warwick, Coventry, CV4 7AL England, United Kingdom*

Lead-based perovskite relaxor ferroelectrics are widely used as materials for numerous applications due to their extraordinary dielectric, piezoelectric, and electrostrictive properties. While the mechanisms of relaxor behavior are disputable, the importance of quenched (static) random electric fields created at nanoscale by the disordered heterovalent cations has been well recognized. Meanwhile, an increasing amount of scientific and technological efforts has been concentrated on lead-free perovskites, in particular, solid solutions of classical ferroelectric BaTiO$_3$ (BT), which better meet ecological requirements. Among BT-based solutions the homovalent systems are elaborately studied where strong random electric fields are absent, while the solubility limit of heterovalent solutions is typically too low to fully reveal the peculiarities of relaxor behavior. In this paper, we prepare a perovskite solid solution system $(1 − x)$Ba^{2+}Ti^{4+}O$_3$−xDy^{3+}Fe^{3+}O$_3$ ($0 \leqslant x \leqslant 0.3$) and study it as a model heterovalent lead-free system. We determine crystal structure, ferroelectric, and dielectric properties of ceramics in a wide range of temperatures and concentrations, construct a phase diagram, and find and analyze the concentration-induced crossover from normal ferroelectric to relaxor behavior. We demonstrate that quenched random electric fields of moderate strength promote the ferroelectric-to-relaxor crossover, but do not change qualitatively the peculiarities of relaxor behavior, while strong enough fields destroy the relaxor state, so that the material becomes an ordinary linear dielectric. The experimental results are compared with the predictions of known theories of relaxor ferroelectricity.

I. INTRODUCTION

In recent years, relaxor ferroelectrics, or relaxors [1,2], have attracted intensive research efforts owing to a rich diversity of extraordinary structural and physical properties and a wide range of technological applications. In particular, lead-containing relaxor ferroelectrics, such as Pb(Mg$_{1/3}$Nb$_{2/3}$)O$_3$−PbTiO$_3$ and Pb(Zn$_{1/3}$Nb$_{2/3}$)O$_3$−PbTiO$_3$, exhibit ultrahigh piezoelectricity and, consequently, can be used as a new generation of acoustic sensors, medical ultrasonic imaging transducers, actuators, and related electromechanical devices [3,4].

Even though lead-based relaxors show excellent physical properties, the development of environmental-friendly lead-free relaxors is in high demand. However, in contrast to lead-based relaxors with record-setting piezoelectricity, the properties of the state-of-the-art lead-free ferroelectrics are still far away from most practical applications. In order to efficiently design and develop high performance lead-free relaxors, it is necessary to understand the physical origin and mechanisms of relaxor behavior. Unfortunately, the knowledge of the underlying mechanisms in lead-free materials is still relatively poor compared to the well-studied lead-containing relaxors [5].

Among several proposed factors influencing the relaxor behavior, random local electric fields related to the underlying structural disorder are often considered to be essential [6–9]. It has been demonstrated recently that strong quenched random electric fields caused by disordered heterovalent cations establish the relaxor phase, identify the order parameter, and cause the dramatic enhancement of piezoelectric coefficients in lead-containing perovskites [9]. Experimental results are consistent with the first-principles-based atomistic simulations showing that random electric fields are necessary to induce relaxor properties in classical relaxor ferroelectric Pb(Mg$_{1/3}$Nb$_{2/3}$)O$_3$ (PMN) [10]. However, some key questions still remain unanswered, such as the following. Is there a critical strength of random field required to induce the relaxor behavior? Will the relaxor characteristics always keep enhancing with the increasing strength of random fields? Do random fields play a similar critical role to determine relaxor behavior in lead-free materials? The last question is especially relevant, as many known lead-free relaxors are homovalent solid solutions where strong random electric fields are absent and, based on the analogy with the lead-containing counterparts, heterovalent modification could be expected to enhance the performance of lead-free materials. On the other hand, atomistic calculations similar to those that predicted the importance of random electric fields in lead-containing

*jzhuang@xjtu.edu.cn
†abokov@sfu.ca
‡zye@sfu.ca

PMN did not reveal any significant influence of random fields on relaxor behavior of lead-free $Ba(Ti_{1-x}Zr_x)O_3$ solid solution [11].

Among the most technologically appealing lead-free perovskite ferroelectrics are solid solution systems $(1 - x)BaTiO_3 - xABO_3$, where A and B are various cations. Of particular fundamental interest are the systems where the second component, ABO_3, is a nonferroelectric, as such systems allow more straightforward theoretical modeling. A number of such relaxors have been formed by homovalent modification of $BaTiO_3$ (BT), including $Ba(Ti_{1-x}Hf_x)O_3$ [12,13], $Ba(Ti_{1-x}Sn_x)O_3$ [14–16], $Ba(Ti_{1-x}Zr_x)O_3$ [17,18], and $Ba(Ti_{1-x}Ce_x)O_3$ [19]. In these systems, with increasing x, the temperature of transition from the paraelectric to ferroelectric (FE) phase (Curie temperature) significantly decreases, the transition progressively becomes more and more diffuse, and the crossover from normal ferroelectric behavior to relaxor behavior is observed at a characteristic concentration, $x_{F-R} \approx 0.2 - 0.3$. The solutions with $x > x_{F-R}$ reveal the features inherent to all (lead-free and lead-containing) relaxors, including a diffuse maximum at T_m in the dielectric permittivity versus temperature dependence, significant frequency dependence of T_m, and macroscopically nonpolar crystal structure below T_m. With further increasing x the relaxor behavior can persist up to the concentration as high as $x \approx 0.8$ and at even higher x a "polar cluster state" has been reported [18].

Many heterovalent BT-based solutions have been already studied, such as $(1 - x)BT - xDyScO_3$ [20], $(1 - x)BT - xBa(Co_{1/2}Nb_{1/2})O_3$ [21], $(1 - x)BT - xBa(Mg_{1/3}Nb_{2/3})O_3$ [22,23], $(1 - x)BT - xLa(Mg_{1/2}Ti_{1/2})O_3$ [24], and $(1 - x)BT - xBa(Sc_{1/2}Nb_{1/2})O_3$ [25]. However, the information about their relaxor properties is comparatively limited, partially because of the difficulties in sample preparation and low solubility limits. The maximum possible concentration of modifiers in these systems does not typically exceed the value of $x = 0.1 - 0.2$, which is only slightly larger than x_{F-R}. Keeping this in mind, in this paper we developed and studied a heterovalent system $(1 - x)BaTiO_3 - xDyFeO_3$ (BT-DF) by introducing a nonferroelectric perovskite $Dy^{3+}Fe^{3+}O_3$ into $Ba^{2+}Ti^{4+}O_3$. Dysprosium orthoferrite, $DyFeO_3$ (DF), is a perovskite oxide which was studied quite long ago as a member of the family of rare-earth orthoferrites exhibiting canted antiferromagnetism and an unusual variety of magnetic properties [26]. Recent revival of interest in this material is related to the multiferroic properties discovered in DF, including the magnetic-field-induced ferroelectric state at very low temperatures [27], the piezoelectromagnetic effect [28], and the coexistence of ferroelectric and magnetic morphotropic phase boundaries in solid solutions between DF and lead-containing ferroelectric $BiFeO_3 - PbTiO_3$ [29,30]. We prepared BT-DF solid solutions in a comparatively large concentration range of $0 \leqslant x \leqslant 0.3$, where heterovalent cosubstitutions on both A and B sites of BT enabled the formation of strong random fields within a comparatively low composition variation, making BT-DF a good model material to study the role of random fields in normal-to-relaxor ferroelectric crossover and relaxor features in lead-free perovskite materials.

II. EXPERIMENTAL DETAILS

A series of $(1 - x)BaTiO_3 - xDyFeO_3$ solid solution ceramics ($x = 0$, 0.01, 0.02, 0.03, 0.04, 0.05, 0.06, 0.08, 0.10, 0.12, 0.14, 0.16, 0.18, 0.20, 0.25, and 0.30) was prepared by solid-state reaction and sintering process. The samples are named according to their compositions, e.g., DF06 stands for $0.94BaTiO_3 - 0.06DyFeO_3$, and so on. The raw materials of $Fe_2O_3(\geqslant99.7\%)$, $Dy_2O_3(\geqslant99.9\%)$, $BaCO_3(\geqslant99.9\%)$, and $TiO_2(\geqslant99.9\%)$ were dried in an oven overnight and weighed in stoichiometric proportions. After mixing with dilute alcohol and hand milling in an agate mortar for 1 h, the mixed powder was dried and pressed into pellets with a diameter of $\Phi = 15$ mm. The pellets were calcined at 1423 K for 6 h on a platinum plate. The calcined samples were then ground thoroughly, mixed with 5% polyvinyl alcohol (PVA), and pressed into pellets with $\Phi = 8$ mm. The pellets were subsequently heated at 873 K for 0.5 h to eliminate the PVA binder and then sintered at higher temperature between 1673 and 1753 K, depending on the composition, for 6 h. The sintered ceramics were crashed and ground into fine powder for x-ray-diffraction (XRD) characterization at room temperature (Bruker D8 Advance diffractometer) as well as at low temperatures (Bruker D5005 diffractometer). The phase components and lattice parameters were calculated based on the Rietveld refinement method using the TOPAS Academic Software package [31]. To characterize the electric properties the ceramic samples were polished and covered with silver electrodes on both circular surfaces to form parallel plate capacitors. The ferroelectric properties were measured by a RT66A Standard Ferroelectric Testing System (Radiant Technologies, Inc.). The complex dielectric permittivity was measured using an impedance analyzer (Novocontrol Turnkey Dielectric Spectrometer Concept) in the temperature range from 123 to 573 K and the frequency range of 1 Hz to 3 MHz. The data were analyzed using the least-square fitting method.

III. RESULTS

A. Phase diagram of the BT-DF system

The crystal structures of all prepared solid solutions have been investigated by XRD at room temperature, as shown in Fig. 1(a). It is evident that the perovskite structure of pure $BaTiO_3$ is preserved as the main component in all studied compositions, indicating the formation of a perovskite solid solution. A very weak diffraction peak appears around 30° for the compositions with $x \geqslant 0.08$, which is marked by an arrow in Fig. 1(a). It belongs most probably to a pyrochlore phase which often appears as a parasitic phase in perovskite ceramics. Additionally, small peaks compatible with the orthorhombic $DyFeO_3$ structure are found for $x \geqslant 0.2$ which become stronger with increasing x, as indicated by the circles. The detailed evolution with composition of the {002} peak in pseudocubic indexing is plotted in the right panel of Fig. 1(a), which shows that two (002) peaks gradually merge into a single peak with increasing x. Note that the small shoulder
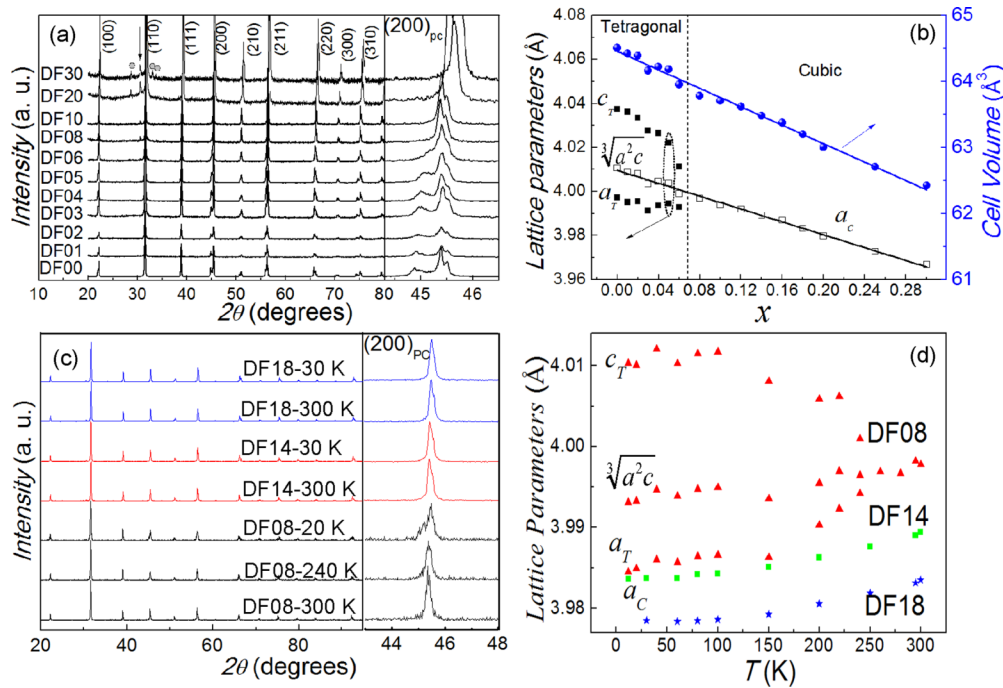
FIG. 1. Room-temperature XRD patterns of different compositions (a), room-temperature composition dependences of lattice parameters and unit-cell volume (b), XRD patterns of selected compositions at different temperatures (c), and temperature dependences of lattice parameters for selected compositions (d) in the $(1-x)$BT$-x$DF system.

on the high-angle side is due to the effect of CuK$_{\alpha 2}$ radiation. This evolution suggests a structural transformation from the tetragonal symmetry of the BaTiO$_3$ origin to the cubic symmetry. The room-temperature Rietveld refinements confirm the phase symmetry change. With increasing DF content, the tetragonal $P4mm$ phase that exists for $x \leqslant 0.06$ transforms to the cubic $Pm\bar{3}m$ phase for $x \geqslant 0.08$. The room-temperature lattice parameters calculated from the Rietveld refinements are plotted in Fig. 1(b). When x increases, the tetragonality (c/a ratio) decreases and approaches the value of unity. The parameter a eventually equals c for the samples with compositions of $x \geqslant 0.08$, which corresponds to the cubic symmetry. As the ionic radius of Fe^{3+} [0.645 Å, 6 coordination number (C.N.)] is smaller than that of Dy^{3+} (0.912 Å, 6 C.N.) and close to the ionic radius of Ti^{4+} (0.605 Å, 6 C.N.), Fe^{3+} is expected to occupy the relatively smaller B sites, and large Dy^{3+} ions enter A sites by substituting Ba^{2+} (1.35 Å, 6 C.N.). As shown in Fig. 1(b), both the lattice parameter a in the cubic phase and the unit-cell volume in the whole concentration range reveal a linear decrease with the increasing amount of DF due to the substitution of the smaller Dy^{3+} for the larger Ba^{2+} ions on the A sites and the smaller Fe^{3+} for the larger Ti^{4+} on the B sites. This linear decrease confirms the formation of the solid solution with x increased up to 0.3 despite the small amount of other phases at high substitution content. The decreasing rate, dV/dx, is found to be ~6.99 Å^3/mol according to the linear fitting results.

Temperature dependences of relative dielectric permittivity (ε) and loss tangent (tanδ) are presented in Fig. 2 for selected compositions. The pure BaTiO$_3$ sample [Figs. 2(a) and 2(b)] shows three permittivity peaks which are known to be related to the cubic-tetragonal, tetragonal-orthorhombic,

and orthorhombic-rhombohedral phase transitions at $T_C = 402$ K, $T_{\text{T-O}} = 291$ K, and $T_{\text{O-R}} = 204$ K, respectively. The peaks are very sharp, revealing the character of normal ferroelectric phase transitions. With 1% substitution of DF, the T_C, $T_{\text{T-O}}$, and $T_{\text{O-R}}$ temperatures decrease to 393, 237, and 160 K, respectively, and the low-temperature dielectric peaks become diffuse as shown in Figs. 2(c) and 2(d). In the DF02 sample, apart from the dielectric peak at $T_C \approx 379$ K, only a very broad anomaly is observed around 195 K, which can be related to the transition from the tetragonal to the low-temperature (orthorhombic or rhombohedral) phase. In DF03 the anomaly becomes even broader and moves to about 150 K [see Fig. 2(e)]. No additional permittivity anomalies besides the peak at $T_m \approx T_C$ can be observed in the studied temperature range for the compositions with $x \geqslant 0.04$. When x increases up to 0.06, T_m remains frequency independent and a more or less sharp drop of ε is observed just below T_m, which is characteristic of the first-order ferroelectric phase transition. At $0.08 \leqslant x \leqslant 0.2$ a significant dispersion of ε appears, leading to the dependence of T_m on frequency which is characteristic of relaxor ferroelectric behavior. At temperatures much larger than T_m the increase of permittivity is evident, which is most pronounced at low frequencies. Such an increase is often observed at elevated temperatures in perovskite materials. It is typically caused by extrinsic polarization mechanisms (Maxwell-Wagner polarization, etc.) and/or contribution of mobile charge carriers [32] and has no relation to ferroelectricity. As one can see in Fig. 2, the loss related to this high-temperature dielectric response behaves in a similar way in BT and all solid solutions, namely, tanδ generally increases with decreasing frequency and, at a given frequency, increases upon heating up to a value of
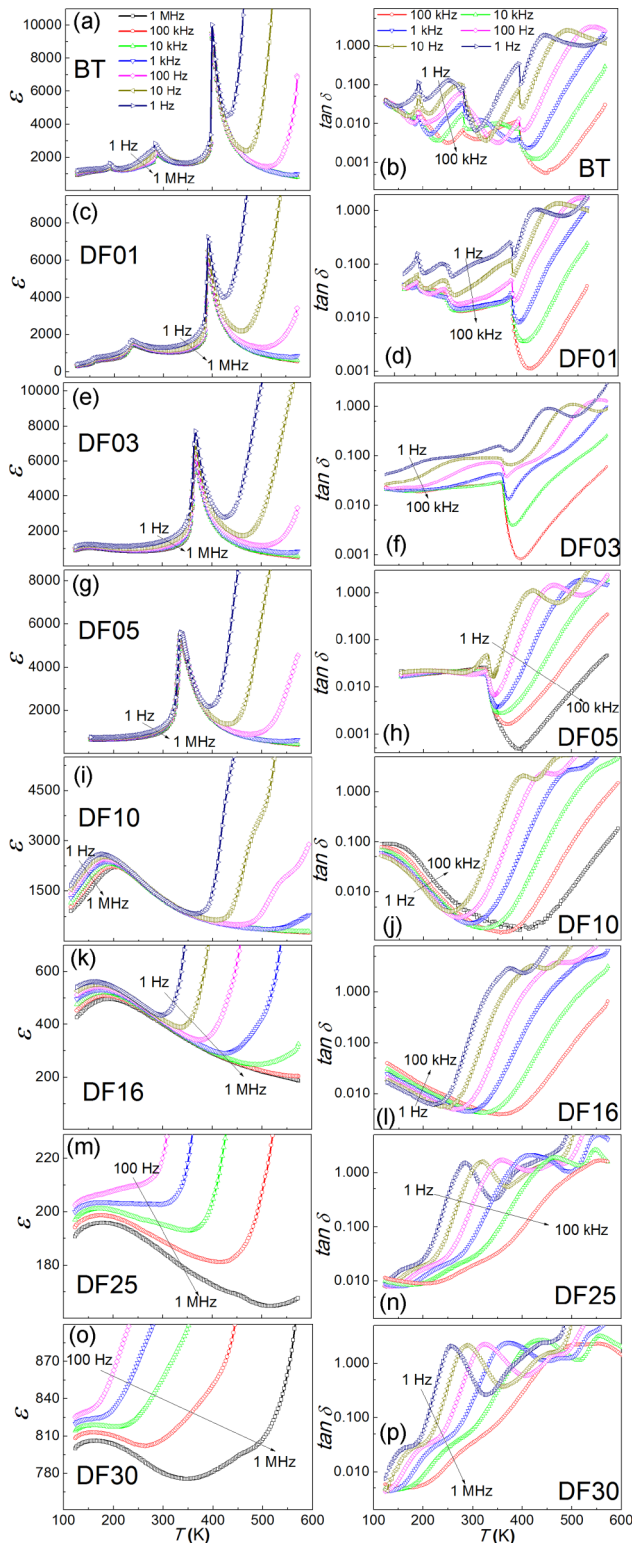
FIG. 2. Temperature dependences of the real part of relative dielectric permittivity and the loss tangent measured upon cooling at different frequencies in selected $(1-x)$BaTiO$_3-x$DyFeO$_3$ compositions: BT (a, b), DF01 (c, d), DF03 (e, f), DF05 (g, h), DF10 (i, j), DF16 (k, l), DF25 (m, n), and DF30 (o, p).

tan$\delta \approx 1$. Then it remains roughly temperature independent in a wide temperature range so that at high enough temperatures and low enough frequencies the frequency dispersion of
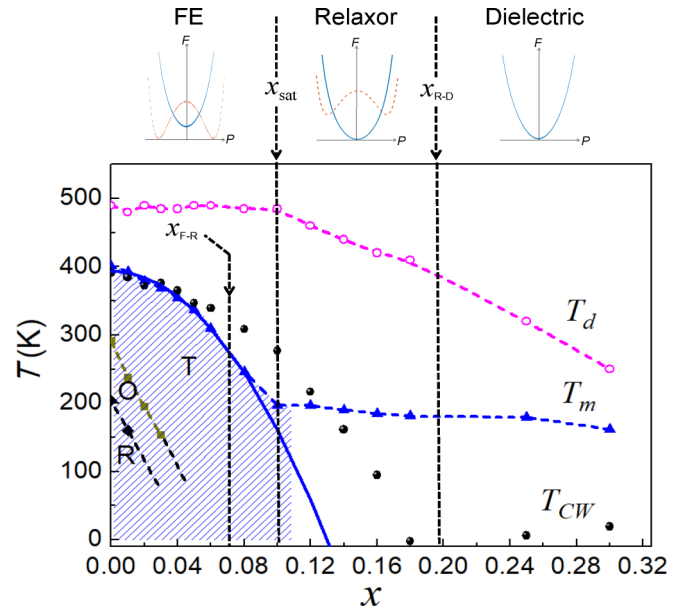

FIG. 3. Phase diagram of the $(1-x)$BaTiO$_3-x$DyFeO$_3$ solid solution system. The shaded area indicates the ferroelectric phase with tetragonal (T), orthorhombic (O), or rhombohedral (R) macroscopic symmetry; in all other areas the symmetry is macroscopically cubic. Composition dependences of the R-O and O-T phase transition temperatures (diamonds and squares, respectively); the temperature of permittivity maximum, T_m (triangles); the Burns temperature, T_d (open circles); and the Curie-Weiss temperature, T_{CW} (filled circles) are presented. The characteristic concentrations x_{F-R}, x_{sat}, and x_{R-D} are indicated. Dashed lines are guides for the eye; the solid line is the fit to Eq. (4) with $T_C(0) = 394$ K and $A = 2.33$ K/mol %. The insets show the low-temperature free energies (F) vs macroscopic polarization (P) for the random field state (solid line) and the FE state (dashed line) in the regions of weak, moderate, and strong random field disorder, respectively, according to the model of Ref. [52].

tanδ practically vanishes. At even higher temperatures tanδ increases again, which can be related to the increased dc conductivity. The frequency-independent tanδ is a sign of so-called low-frequency dispersion (LFD) which is related to mobile charge carriers [32,33]. This dispersion follows the universal relaxation law, with both the real and imaginary parts of permittivity being proportional to f^{n-1} and the frequency-independent tanδ depending on the value of parameter n [8,31]. We conclude, therefore, that at high temperatures the dielectric response of all the studied solid solutions is dominated by the universal relaxation with approximately the same parameter n, while at lower temperatures the ferroelectric polarization with corresponding permittivity peak becomes dominating. The magnitude of this peak decreases with increasing x so that at $x \geqslant 0.2$ the LFD not related to ferroelectricity becomes important even in the range of T_m.

The behavior of T_m determined at 100 kHz (where the contribution of nonferroelectric polarization to the permittivity is negligible) is shown in Fig. 3. In compositions with $x \leqslant 0.06$, T_m evidently corresponds to the temperature of cubic-tetragonal phase transition, as the room-temperature structure remains tetragonal [see Fig. 1(b)] and no dielectric anomalies corresponding to a phase transition are observed

between room temperature and T_m. To determine the structures at larger x we performed additional low-temperature XRD investigations. The DF08, DF14, and DF18 samples were studied in the temperature range from room temperature down to 12 K, which covers the dielectric maximum temperature, T_m. Figure 1(c) shows the XRD patterns at selected temperatures. Obvious splitting and broadening are seen in {002} peaks for DF08 at all temperatures below $T_m = 250$ K, indicating a noncubic structure which is, however, not a rhombohedral one in contrast to the lowest-temperature phase of the pure BT. To establish the phase symmetry of DF08 at low temperature, orthorhombic, rhombohedral, and tetragonal phases (i.e., the phases observed in pure BT) were tested to fit the XRD pattern at 20 K. The tetragonal model with $P4mm$ symmetry gives the best fitting results and, therefore, has been assigned to the low-temperature phase of DF08. In the DF14 and DF16 samples the cubic phase remains at all investigated temperatures. The calculated lattice parameters are shown in Fig. 1(d). For both compositions lattice parameter a continuously increases with temperature, as expected for a normal thermal expansion.

To complete the macroscopic structure-composition diagram of the $(1 - x)\mathrm{BT} - x\mathrm{DF}$ system, the low-temperature transitions ($T_{\text{T-O}}$ and $T_{\text{O-R}}$) determined from the dielectric measurements are also shown in Fig. 3. Similar to most other BT-based solid solutions with a nonferroelectric second end member, in the BT-DF system investigated here, $T_m \approx T_c$ significantly decreases with increasing x. The behavior of the T-O and O-R transitions can, however, be different in different systems. The decrease of T_m is often accompanied by the increase of both $T_{\text{T-O}}$ and $T_{\text{O-R}}$, and the lines of three phase transitions in a phase diagram merge at a certain concentration [34] (this is sometimes called a "pinching" effect). Simultaneous decrease of all transition temperatures which we observe in BT-DF is another frequent possibility which has been observed, e.g., in the $\mathrm{BT} - \mathrm{DyScO_3}$ system [20].

While T_m initially decreases with increasing x, when the concentration of DF reaches $x_{\text{sat}} \approx 0.1$, the decrease terminates, and at larger concentrations T_m becomes practically composition independent (Fig. 3). Similar $T_m(x)$ saturation is usually observed in BT-based relaxor systems with homovalent substitutions including $\mathrm{Ba(Ti_{1-x}Zr_x)O_3}$ [18], $\mathrm{Ba(Ti_{1-x}Sn_x)O_3}$ [15], $\mathrm{Ba(Ti_{1-x}Ce_x)O_3}$ [19], and

$\mathrm{Ba(Ti_{1-x}Hf_x)O_3}$ [13]. In those cases, $x_{\text{sat}} = 0.3 - 0.4$ was found, which is significantly larger than the solubility limit of most known BT-based heterovalent solutions in which the second ABO_3 component is not a ferroelectric. This is presumably the reason why the saturation was not previously observed in such heterovalent systems.

B. Ferroelectric-to-relaxor crossover in the BT-DF system

The results of the previous section suggest that the BT-DF compositions with large enough concentrations of DF possess the properties characteristic of relaxors. Indeed, we reveal key relaxor characteristics in these samples, namely, a large and diffuse permittivity peak, the temperature of which shifts with frequency and the macroscopically cubic structure at all temperatures above and below this peak. Therefore, a crossover from a normal ferroelectric behavior (at small x) to a relaxor ferroelectric behavior (at larger x) is observed in the BT-DF system similar to many other BT-based solids solutions. In the present section we analyze the crossover in detail.

While the behavior of ε around T_m remains similar at all ferroelectric compositions with $x \leqslant 0.06$ (sharp peak without significant dispersion and the dispersion in the ferroelectric phase), the loss shows significant variation [Figs. 2(a)–2(h)]. In pure BT the value of $\tan\delta$ dramatically decreases with increasing frequency. This dispersion is known to be related mainly to the relaxation of domain walls [35]. It decreases gradually with increasing x and at $x \approx 0.05$ the temperature- and frequency-independent $\tan\delta \approx 0.02$ is observed below T_m [Fig. 2(h)]. This suggests a dramatic evolution of ferroelectric domain structure with composition. In the samples with $x \geqslant 0.06$ the behavior is qualitatively different. In a wide temperature range around T_m, $\tan\delta$ is the increasing function of frequency, which implies the development of a (conventional relaxor) relaxation mechanism not found in the samples with smaller x. Figure 2(j) demonstrates the diffuse $\tan\delta$ (T) maximum observed in DF10 slightly below T_m which shifts with frequency similar to T_m. This behavior is also characteristic of relaxors. Note that the maximum value of $\tan\delta$ (T) ≈ 0.1 is identical to that observed in the classical relaxor PMN [1]. However, larger concentrations of DF provoke other qualitative changes: the characteristic relaxor relaxation decreases with increasing x and practically vanishes at $x > 0.2$.
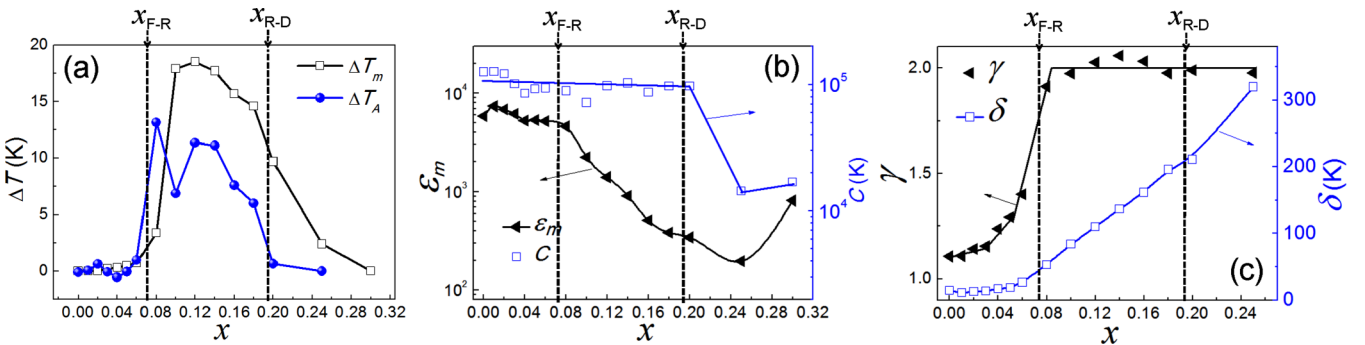

FIG. 4. Composition dependences of the parameters characterizing the ferroelectric state in the $(1 - x)\mathrm{BaTiO_3} - x\mathrm{DyFeO_3}$ solid solutions: the frequency shift of permittivity maximum, $\Delta T_m = T_m$ (1 MHz) $- T_m$ (100 Hz) (open squares) and the difference $\Delta T_A = T_m - T_A$ at 100 kHz (solid spheres) (a); the magnitude of permittivity maximum, ε_m, at 100 kHz (solid triangles) and the Curie constant, C (open squares) (b); and the parameters of Eq. (3), δ (open squares) and γ (solid triangles) (c). The lines are guides for the eye.
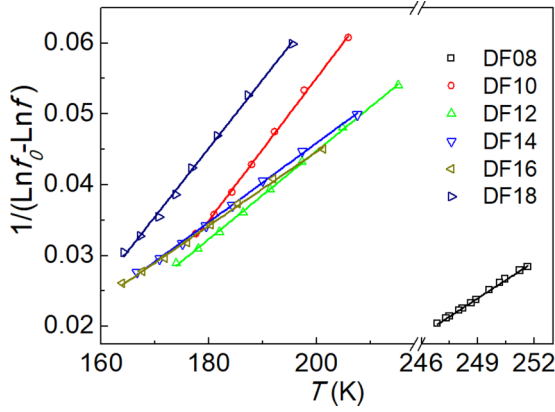
FIG. 5. The Vogel-Fulcher fitting for the $(1-x)\text{BaTiO}_3-x\text{DyFeO}_3$ compositions with $0.08 \leqslant x \leqslant 0.18$.

To describe the relaxor dispersion qualitatively we plot in Fig. 4(a) the difference, $\Delta T_m = T_m(1\,\text{MHz}) - T_m(100\,\text{Hz})$, characterizing the rate of T_m variation with frequency. This parameter is often used to determine the concentration range of the relaxor phase in solid solutions. At small x, ΔT_m remains practically zero, but above $x_{\text{F-R}} \approx 0.07$ a sharp increase is observed, signifying the crossover from the normal ferroelectric to relaxor behavior. Interestingly, with further increase in x, ΔT_m tends to zero again, which is evidently due to the vanishing of characteristic relaxor relaxation mentioned in the previous paragraph. Therefore, the hallmark of relaxor behavior, i.e., the frequency shift of T_m, is absent in ceramics with large x and those samples cannot be classified as relaxors. Similar vanishing of the $T_m(f)$ dispersion, which signifies a disappearance of relaxor behavior, has not been reported so far in BT-based solid solution systems to the best of our knowledge. In some cases this is probably because the solubility limit is reached before this happens.

The empirical Vogel-Fulcher (VF) law can be applied to characterize the frequency dispersion of T_m in relaxors [36]:

$$f = f_0 \exp\left[-\frac{E_a}{k(T_m - T_{\text{VF}})}\right], \qquad (1)$$

where f is the measurement frequency, and E_a, T_{VF}, and f_0 are the parameters. The VF model fittings for different relaxor compositions are shown in Fig. 5. It can be seen that T_m fits the VF law in the range of $0.08 \leqslant x < 0.2$, confirming the relaxor nature of these compositions. The fitting parameters are listed in Table I. In canonical relaxors, T_{VF} is often close

to the freezing temperature of the relaxation spectrum, T_f, at which the characteristic relaxation time diverges and f_0 is the attempt frequency of dipolar dynamics which is of the order of phonon frequency ($\sim 10^{13}$ Hz). However, in some relaxors, in particular, in lead-free ones, T_{VF} can be significantly different from and usually higher than T_f, and f_0 does not correspond to the attempt frequency [32,37]. The fact that f_0 in most BT-DF compositions is far away from the possible phonon frequency range suggests that T_{VF} is not an actual freezing temperature.

It is known that in both normal ferroelectrics and relaxors the static dielectric permittivity (ε_S) in the paraelectric phase can be described by the Curie-Weiss (CW) law:

$$\varepsilon_s = \varepsilon_\Delta + \frac{C}{T - T_{\text{CW}}}, \qquad (2)$$

where T_{CW} is the Curie-Weiss temperature, C is the Curie constant, and ε_Δ is the parameter which represents possible temperature-independent nonferroelectric polarization mechanisms (e.g., a contribution of hard optic phonons or extrinsic dielectric contributions) [32,38]. We verify this law using the data in the frequency range of 100 kHz to 3 MHz, where the extrinsic contribution from mobile charge carriers (which decreases with increasing f) is small in the relevant temperature range and the measured data represent the static ferroelectric permittivity. As shown in Fig. 6, the CW law is well satisfied above the temperature T_d, which is conventionally associated with the so-called Burns temperature in relaxors. It is often believed that upon cooling from the high-temperature paraelectric phase the local dynamic polar nanoregions start to appear at T_d, leading to the formation of the ergodic relaxor state. In order to obtain the exact values of T_d the fitting residuals, $(\varepsilon_{\text{cal}} - \varepsilon)/\varepsilon$ (where ε_{cal} is the calculated value given by the CW law with the best-fit parameters), are analyzed as shown in Fig. 6(b). The concentration dependence of T_d determined in this way is shown in Fig. 3. In the range of $0 \leqslant x \leqslant 0.1$, T_d remains practically the same as in pure BT (≈ 490 K). This behavior is not unexpected: the composition-independent T_d has been observed in other systems in a wide range of $x \geqslant 0$, e.g., in BT−BiScO$_3$ and BT−BaSnO$_3$ [15,39]. At $x > 0.1$, the T_d value decreases monotonously down to ≈ 250 K in the DF30 sample. The best-fit values of ε_Δ are found to be practically zero for $x \leqslant 0.02$, in the range of 0–60 for $0.03 \leqslant x \leqslant 0.2$ and 720 at $x = 0.3$, which is in agreement with the fact that the contribution of mobile charge carriers not related to the CW mechanism becomes significant at large

TABLE I. Fitting parameters of the Vogel-Fulcher law, Eq. (1), for the compositions with $0.08 \leqslant x \leqslant 0.18$.

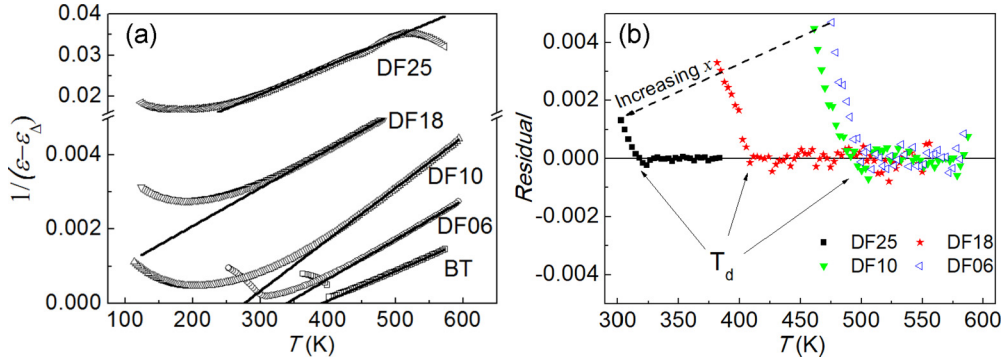| Parameter x	0.08	0.10	0.12	0.14	0.16	0.18
f_0 (Hz)	1.97×10^{21}	1.41×10^{13}	1.10×10^{15}	5.10×10^{15}	4.32×10^{16}	1.79×10^{14}
E_a (eV)	0.05	0.086	0.139	0.155	0.165	0.089
T_{VF} (K)	235	145	128	118	114	133

FIG. 6. The Curie-Weiss law for the $(1-x)BaTiO_3 - xDyFeO_3$ solid solution system. The fitting to Eq. (2) (a) and the corresponding residuals (b) for selected compositions.

x. The Curie constant decreases slightly from 1.25×10^5 K in BT to 0.97×10^5 K in DF20 and then drops by an order of magnitude, as shown in Fig. 4(b).

The behavior of T_{CW} is of particular interest because in normal ferroelectrics T_{CW} is observed at or below T_m, while in relaxors the relation $T_{CW} > T_m$ typically holds. In the BT-DF system T_{CW} decreases with increasing *x*, starting from 391 K in BT (see Fig. 3), but the decrease is slower than the T_m decrease so that at $x \geqslant x_{F-R}$ the behavior characteristic of relaxors is observed, confirming the ferroelectric to relaxor crossover. However, at higher *x* the value of T_{CW} becomes smaller than T_m again and reaches the value of 0 K at $x \geqslant$ 0.18, suggesting that the BT-DF compositions with large *x* are not relaxor ferroelectrics. Furthermore, they are apparently not ferroelectrics at all, in spite of the existence of the $\varepsilon(T)$ maximum at $T_m \approx 170$ K. Indeed, the magnitude of the maximum (ε_m) in DF25 is as small as $\varepsilon_m \sim 200$ [see Fig. 4(b)] which is characteristic of ordinary dielectrics rather than perovskite ferroelectrics (larger ε_m in DF30 evidently originates from mobile charge carriers' dielectric contribution). T_{CW} is known to be the temperature below which the paraelectric phase becomes unstable, thus zero T_{CW} observed at $x \geqslant 0.18$ allows the existence of the paraelectric phase at all nonzero temperatures. The value $T_{CW} = 0$ is theoretically predicted for the relaxation in a system of noninteracting dipoles [40]; noninteracting dipoles imply the absence of ferroelectric-type or dipole glass-type states. To interpret the behavior $\varepsilon(T)$ in BT-DF with large *x*, note that Wang *et al.* [41,42] found recently, using first-principles-based molecular dynamic simulations, that in $Ba(Ti_{0.5}Zr_{0.5})O_3$ the dielectric response originates mainly from the reorientations of the dipole moments of individual and weakly interacting Ti-containing unit cells and the correlation length of interactions is so small that the FE order cannot be established. It was found to lead to the diffuse maximum in the temperature dependence of permittivity at $T_m \sim 150$ K, having the amplitude of $\varepsilon_m \sim 250$ and dielectric dispersion in the gigahertz range. The values of ε_m and T_m observed in BT-DF at $x \geqslant 0.20$ are consistent with those calculated values, thus the $\varepsilon(T)$ maximum probably has the same origin.

To describe analytically the high-temperature slope of the diffuse $\varepsilon(T)$ peak observed in relaxors at $T < T_d$, several empirical expressions have been proposed [32,43–46]. We use here the most general one which includes the others as

particular cases:

$$\frac{\varepsilon_A}{\varepsilon} = 1 + \frac{|T - T_A|^\gamma}{2\delta^\gamma}. \tag{3}$$

This equation represents a bell-shaped $\varepsilon(T)$ peak where T_A and ε_A are the position and the height of the peak, respectively, and the diffuseness parameter δ equals the half width of the peak at 2/3 of its maximum. With $\gamma = 2$ Eq. (3) is reduced to the Lorenz function. In both classical lead oxide relaxors and lead-free relaxor systems the measured $\varepsilon(T)$ typically fits Eq. (3) in the temperature range between $T_1(>T_m)$ and $T_Q(<T_d)$ with $\gamma = 2$ and $T_A < T_m$ [8,15,32,46]. However, applicability of this equation in the composition range of ferroelectric-to-relaxor crossover of BT-based heterovalent systems has not been tested so far to the best of our knowledge.

Our results confirm the validity of Eq. (3) for all studied BT-DF compositions. The examples are demonstrated in Fig. 7. Figure 4(c) shows the best-fit parameters δ and γ as functions of composition. The parameters are reported for frequencies of 100 kHz or 1 MHz, but they are evidently frequency independent in the whole frequency range where significant dispersion is absent. Interestingly, Eq. (3) is satisfied (with $\gamma = 1.113 \pm 0.006$ and $T_A = T_m$) even in classical ferroelectric BT. This is, however, consistent with the fact that
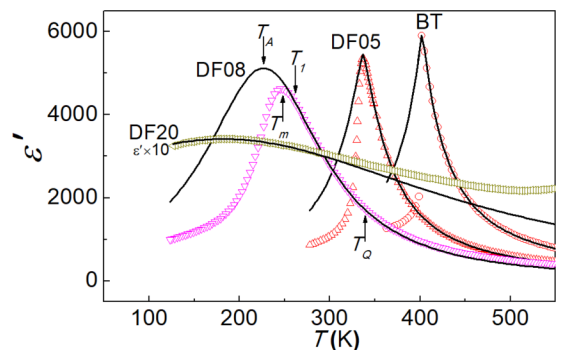

FIG. 7. Fitting of the temperature dependences of permittivity measured at 100 kHz to Eq. (3) for the $(1-x)BaTiO_3 - xDyFeO_3$ compositions with $x = 0, 0.05, 0.08$, and 0.2. For sample DF08 the characteristic temperatures T_A, T_m, T_1, and T_Q are marked.
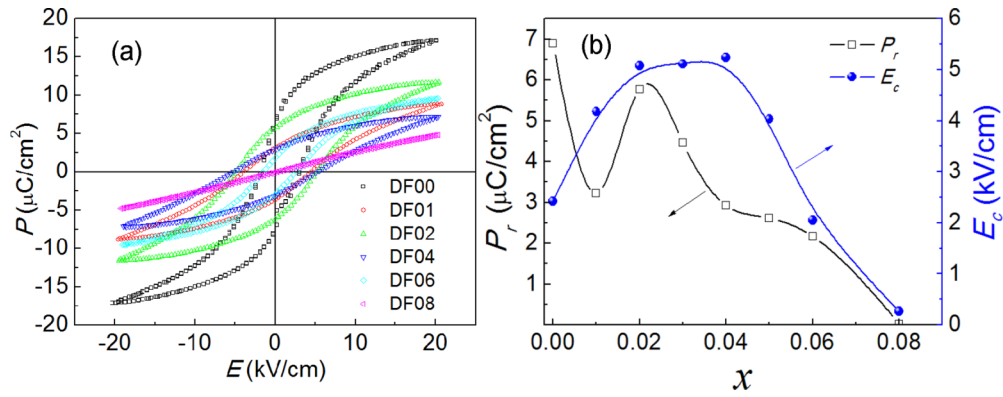
FIG. 8. Ferroelectric properties of the $(1 - x)$BT$-x$DF solid solutions. The polarization-electric field hysteresis (P-E) loops measured at 1 Hz in different compositions at room temperature (a) and dependences of remanent polarization and coercive field at room temperature (RT) on composition (b).

the CW law [which is the same as Eq. (3) with $\gamma = 1$] holds in BT only at $T > T_d$.

The temperature T_Q below which Eq. (3) holds is typically located at about 100 K above T_m, as Fig. 7 illustrates. The temperature T_1, below which this equation is violated, behaves differently for different compositions. At $x \leqslant 0.06$ the difference $T_1 - T_m$ is positive and does not exceed several degrees Kelvin. At $x \geqslant 0.2$ it is negative (e.g., $T_1 - T_m \approx -25$ K in DF25), that is, Eq. (3) correctly describes the experimental data not only above but also below the peak temperature, T_m. In the range of relaxor compositions, $0.08 \leqslant x < 0.2$, T_1 is located at about 20 K above T_m. Such behavior of T_1 is reasonable, as Eq. (3) is known to describe the dependence of static relaxor permittivity. The deviation of experimental data from this equation at $T < T_1$ is due to the development of conventional relaxor dispersion. This dispersion is absent in nonrelaxor solid solutions with $x \geqslant 0.2$ in which we measure, both below and above T_m, the static permittivity, ε_s, of the polarization mechanism, responsible for the $\varepsilon(T)$ maximum plus the susceptibility of mobile charge carriers. The latter susceptibility decreases with increasing frequency and at ~ 1 MHz becomes negligible around T_m. Based on the above explanation, another parameter conveniently describing the relaxor dispersion as well as ferroelectric-to-relaxor and relaxor-to-dielectric crossovers can be introduced, namely, $\Delta T_A = T_m - T_A$. The dependence of ΔT_A on x is shown in Fig. 4(a). Similar to ΔT_m, nonzero values of ΔT_A in this figure clearly mark the interval of relaxor compositions, $0.07 \approx x_{\text{F-R}} \leqslant x \leqslant x_{\text{R-D}} \approx 0.2$.

The boundary concentrations $x_{\text{F-R}}$, x_{sat}, and $x_{\text{R-D}}$ can also be seen in the dependences of other parameters on x. The anomaly in the $\varepsilon_m(x)$ plot is observed at $x_{\text{F-R}}$, while a significant change of the Curie constant corresponds to $x_{\text{R-D}}$ composition [Fig. 4(b)]. The concentration x_{sat} separates the regions where T_d is constant and where it decreases with increasing x (Fig. 3). The increase with x of the diffuseness coefficient, δ, is quite slow at $x > x_{\text{F-R}}$ (from $\delta = 13$ K in BT to $\delta = 19$ K in DF05), while, at $x > x_{\text{F-R}}$, $\delta(x)$ increases rapidly [Fig. 4(c)]. The shape parameter, γ, grows sharply at $x_{\text{F-R}}$ and at all concentrations above $x_{\text{F-R}}$ adopts practically the same value, $\gamma = 2$, which is characteristic of relaxors. Qualitatively similar $\delta(x)$ behavior has been observed in the homovalent

Ba(Ti$_{1-x}$Sn$_x$)O$_3$ solid solution system [15]. However, in that system the value of $\gamma = 2$ has been found not only at $x > x_{\text{F-R}}$ but also in some concentration range below $x_{\text{F-R}}$.

Normal ferroelectrics and relaxors can also be distinguished based on their response to a reasonably high electric field. Therefore, the ferroelectric properties of different compositions are investigated under applied ac electric fields up to 20 kV/cm, and the resulting polarization (P)–electric-field (E) relations are presented in Fig. 8. At room temperature the pure BT shows a typical ferroelectric hysteresis loop with a remanent polarization of $P_r = 6.9 \, \mu$C/cm^2, which agrees with the literature data, while the DF08 sample with the cubic symmetry at room temperature demonstrates an almost linear behavior [Fig. 8(a)]. The variations of coercive field (E_c) and P_r with composition at room temperature are plotted in Fig. 8(b). The value of P_r generally shows a decrease with increasing x, which is consistent with the above discussed decreasing Curie temperature and tetragonality. Note, however, that the DF01 sample shows a significantly smaller P_r as compared to DF00 and DF02. The coercive field demonstrates an increase with the increasing content of DF until $x = 0.02$, which can be attributed to two causes: (i) the increase of the concentration of lattice defects created by the Dy^{3+} and Fe^{3+} ions which inhibit the domain-wall motion and (ii) the fact that the material gets farther away (in temperature) from the (T-O) phase transition. The compositions with $x > 0.04$ show decreasing E_c with increasing x. This is because the material gets closer in temperature to the Curie point.

In order to investigate the evolution of ferroelectric ordering with temperature, three representative compositions, namely, DF08 with x between $x_{\text{F-R}}$ and x_{sat}, DF14 with x between x_{sat} and $x_{\text{R-D}}$, and DF25 with $x > x_{\text{R-D}}$, are chosen to measure the $P(E)$ loops at different temperatures upon heating in the wide temperature range including T_m. As shown in Fig. 9(a), for the DF08 sample the ferroelectric hysteresis loop is observed at low temperatures (with $P_r = 3.9 \, \mu$C/cm^2 at 213 K) confirming that the tetragonal phase revealed in XRD experiments is ferroelectric. The loop gradually becomes slim as the temperature goes up. The variations of P_r and E_c with temperature are plotted in Fig. 8(b). The remanent polarization decreases gradually when approaching $T_m \approx 245$ K from below, signifying a transition from ferroelectric to ergodic
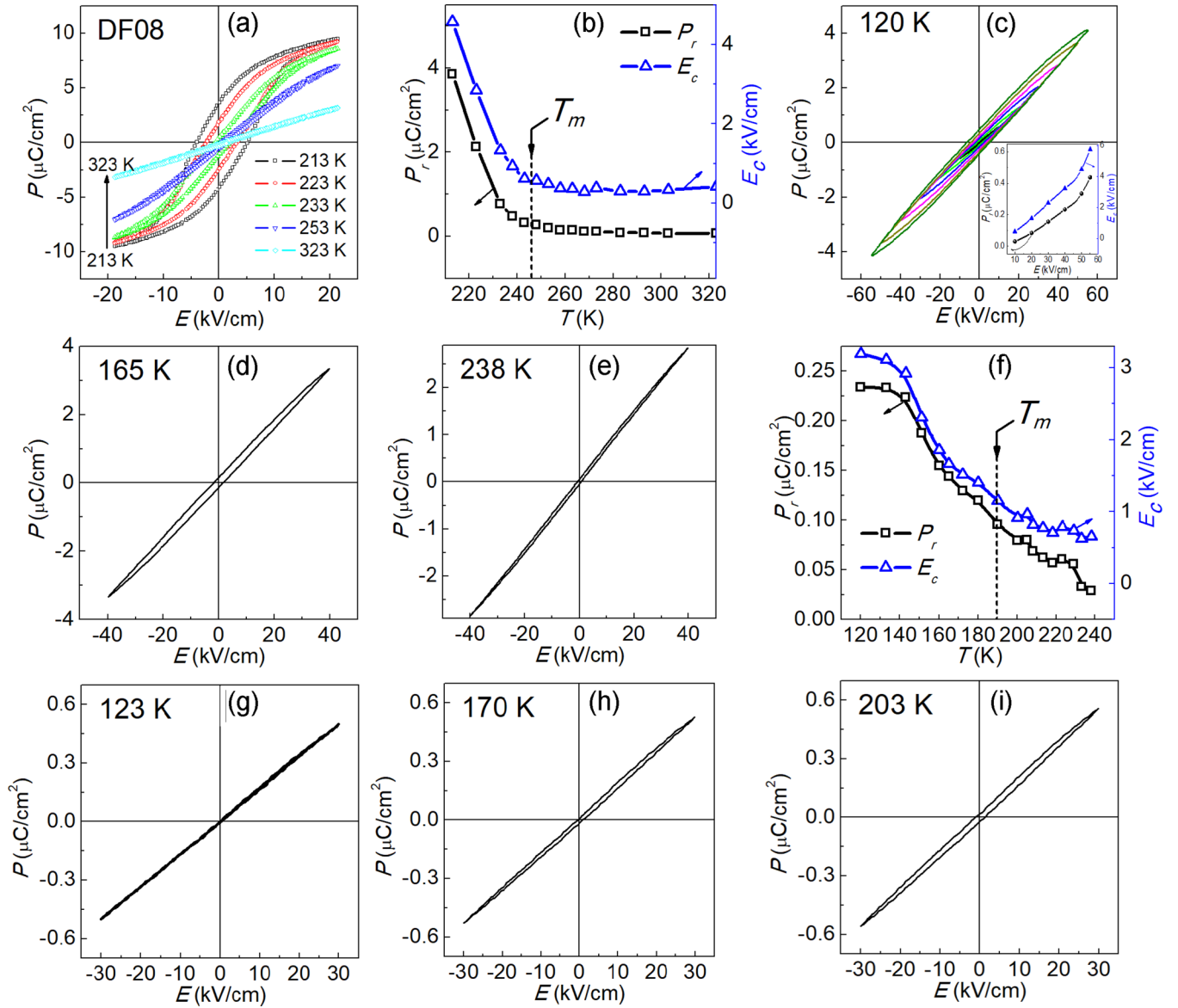
FIG. 9. The P(E) loops measured at different temperatures in DF08 (a) and dependences of remanent polarization and coercive field on temperature in DF08 (b). The P(E) loops measured in DF14 at 120 K (c), 165 K (d), and 238 K (e) and dependences of measured remanent polarization and coercive field on temperature in DF14 (f). The P(E) loops measured in DF25 with the maximal field of 30 kV/cm at selected temperatures: 123 K (g), 165 K (h), and 238 K (i). The measured remanent polarization and coercive field as functions of applied electric field in DF14 at 120 K are plotted in the inset of panel (c).

relaxor state. A small but noticeable "tail" of P_r is observed in the temperature range of several dozen degrees Kelvin above T_m. Such a kind of behavior is typical of lead-oxide relaxor ceramics [1] and relaxor compositions of homovalent BT-based systems [47].

For the DF14 sample in which a macroscopically cubic state is found with XRD at all temperatures, slim hysteresis loops are observed [Figs. 9(c)–9(e)] characteristic of classical relaxors at temperatures around $T_m \approx 190$ K [1]. As Fig. 9(c) demonstrates, the loops are far from being saturated, so that the measured values of P_r and E_c increase with increasing maximal field and, therefore, do not fully characterize the polar state. Because of the electrical breakdown, it was not possible to study the samples at higher fields. Note that similar behavior can be observed due to significant leakage current

even in linear dielectrics with enhanced dc conductivity, which is characteristic of many Fe-containing perovskites because of the coexistence of Fe^{2+} and Fe^{3+} ions [48]. However, the conductivity of dielectrics always increases on heating and the related loop should become wider. We found the opposite behavior: measured values of P_r and E_c decrease and tend to vanish at $T > T_m$ as shown in Fig. 9(f). Therefore the hysteresis loops observed in DF14 can be safely related to the formation of the field-induced polar state that remains after the field is removed. However, we do not have enough information to conclude unambiguously whether this state is stable (and, therefore, nonergodic) or metastable (in this case, the question of ergodicity remains open) and to discuss the possible differences of this state in BT-DF and other relaxors. In particular, in PMN the field-induced

phase is truly ferroelectric and XRD experiments confirm the noncubic symmetry, while in Ba(Ti$_{1-x}$Zr$_x$)O$_3$ relaxors it remains cubic according to XRD (such a state was called quasiferroelectric) [49].

For the DF25 sample, the linear $P(E)$ dependence holds for all the temperatures investigated, even much lower than $T_m \approx 180$ K, as shown in Figs. 9(g)–9(i). This observation confirms the conclusion that the compositions with $x > x_{R-D}$ are ordinary dielectrics. A minor hysteresis which appears at comparatively high temperatures can be attributed to the contribution of enhanced dc conductivity.

IV. DISCUSSION

We have found therefore that in the BT-DF heterovalent solid solution system a gradual increase of DF concentration results in the decrease of the Curie temperature and crossover at a concentration $x_{F-R} \approx 0.07$, from the behavior characteristic of normal ferroelectrics to the relaxor ferroelectric behavior. At concentration $x_{R-D} \approx 0.2$ another crossover is observed from relaxor compositions to the compositions showing nonrelaxor and nonferroelectric behavior. In other BT-based heterovalent systems, close x_{F-R} values are typically observed [20–25,50,51], but homovalent modifications of BT always result in much larger x_{F-R} and x_{R-D} [13,15,18,19]. We attribute this difference to the influence of quenched (static) local fields which must appear in the perovskite solid solution structure due to random distribution of differently charged cations over equivalent lattice sites (Ba^{2+} and Dy^{3+} cations on A sites and Ti^{4+} and Fe^{3+} cations on B sites). It is known that FE ordering occurs due to electrostatic dipole-dipole interactions. The interactions create a spontaneous internal molecular field which aligns individual local dipoles existing in the structure. Being added to the field of dipole-dipole interactions, quenched random fields may disrupt the alignment of dipoles. Such a scenario has been recently demonstrated by Arce-Gamboa and Guzmán-Verri within a statistical mechanical solution of a minimal microscopic model [52]. The considered model Hamiltonian contained, besides the standard single-site and dipole-dipole interaction energy terms which are necessary to reproduce a FE transition, an additional term describing the energy of the interaction between local (dynamic above the Curie temperature) dipoles and static normally distributed random field with zero mean and variance Δ. As the symmetry of the Hamiltonian is cubic, the model may physically correspond to a perovskite ferroelectric solid solution in which positionally disordered cations have similar size, mass, and chemical bonding, but different charge, while the parameter Δ which characterizes the quenched random field strength equals zero in unmodified ferroelectrics (BT in our case) and increases with increasing x. In the T-x phase diagram the theory identifies three regions according to the quenched random fields strength. While Δ is small, and fields are weak as compared to the molecular field responsible for FE ordering, T_C decreases in proportion with Δ^2 and a macroscopically nonpolar "random field" state appears at low temperatures but remains metastable. Assuming that $\Delta \propto x$ in this region we obtain

$$T_C = T_C(0) - Ax^2, \qquad (4)$$

where $T_C(0)$ is T_C at $x = 0$ and A is a constant. In agreement with this prediction, T_m in the BT-DF system (which equals T_C at small x according to XRD data), can be well fitted to Eq. (4), as shown in Fig. 3. Therefore, the model region of weak random fields corresponds to the composition region of the BT-DF system between $x = 0$ and $x \approx x_{sat}$. Note that homovalent modification of BT typically results in linear or almost linear $T_C(x)$ decrease at $x < x_{F-R}$ [12,15,18,19,53], thus the quadratic dependence observed in BT-DF can be attributed exclusively to the influence of random field.

In the range of moderate quenched random fields, the theory predicts at low temperatures a metastable long-ranged polar state and a stable random field state. This agrees with our observations for $x_{sat} < x < x_{R-D}$. Indeed, the macroscopically nonpolar zero-field cooling state is found in this range by XRD, while slim hysteresis loops are in agreement with the existence of a metastable polar state. For the range of strong random field disorder, the polar state theoretically becomes unstable and only the random field state remains. Accordingly, at large x we do not observe $P(E)$ hysteresis in BT-DF even below T_m.

Though the composition- and temperature-induced phase sequences found in the BT-DF system are compatible with the theoretical predictions of the minimal cubic random field microscopic model [52], the experimental dielectric results are reproduced by the theory only partially. The increase of both Δ (in theory) and x (in experiment) leads to a significant decrease of the maximal static dielectric constant. However, the discrepancy is evident in the $\varepsilon_s(T)$ shape at large x. Theoretical $\varepsilon_s(T)$ dependences at $\Delta \neq 0$ demonstrate a monotonous increase with decreasing temperatures (see the inset in Fig. 3 of Ref. [52]). The static permittivity was theoretically calculated from the polarization correlation length and, therefore, corresponds to an experimentally measured small signal ε_s. We found in BT-DF solutions with $x > x_{R-D}$ the maximum in the temperature dependence of small-signal ε_s (at T_m) in contrast to the theory.

As discussed throughout the previous section, the relaxor features caused by heterovalent substitutions (accompanied by strong random fields) and by isovalent substitutions (without such fields) are qualitatively similar, though observed in different concentration ranges. This suggests that in BT-DF microscopic mechanisms other than strong quenched fields may exist that lead to relaxor ferroelectric behavior. The discussed above deviation of static permittivity from the trend prescribed by the random field theory may be due to these mechanisms. Indeed, the static permittivity maximum in homovalent Ba(Ti$_{1-x}$Zr$_x$)O$_3$ relaxor compositions has been found both in experiments [49] and by atomic simulations [42].

Several approaches and models have been proposed to explain the origin of the relaxor state in the case of homovalent disorder, such as (i) the suggestion that it originates from local random strains [54], (ii) the model proposed by Westphal, Kleemann, and Glinchuk [6] based on Imry-Ma theory [55] which allows breaking the long-range order in an arbitrary weak quenched random field, and (iii) the soft pseudospin glass model which takes into account the site and bond disorder, but ignores quenched random fields and strains [56]. In heterovalent BT-DF solid solutions some of

those mechanisms probably also contribute to the disruption of long-range FE order. We can hardly assess the importance of each of them based on the results of our measurements, but we can recall that, according to the first-principles-based simulations [11], turning off random fields and random strains does not significantly affect the relaxor behavior in homovalent $Ba(Ti_{0.5}Zr_{0.5})O_3$. We conclude, therefore, that the above-considered mechanisms i and ii are not important in BT-based systems and the most probable mechanism is related to the effect of substitution of ferroactive Ti cations by Fe cations the contribution of which to ferroelectricity is less significant. It is known [57,58] that the hybridization (covalent bonding) between electronic $3d$ states of Ti^{4+} ions and $2p$ states of O^{2-} ions reduces the short-range interionic repulsion and helps thereby the dipole-dipole interactions to build up the spontaneous polarization in BT. The electronic states of ions with d electrons, such as Fe^{3+}, are unlikely to be hybridized with $2p$ O^{2-} states [59] and, therefore, they are not expected to be ferroactive. The effect of homovalent dilution of Ti ions in BT has been studied in the frame-work of the soft pseudospin glass microscopic model [60], which considers the model Hamiltonian with randomly placed lattice sites of two types populated by Ti and modifying cations, respectively. The model also takes into account the frustration of interactions caused by quenched compositional disorder (the relaxor phase is termed "pseudospin glass" in that work because of the analogy with the magnetic alloys). The model predicts the maximum in temperature dependence of small-signal permittivity in relaxor composition, in contrast to the conclusions of the above-considered strong random field model [52] and in agreement with our observations for BT-BF. However, the maximum is predicted to have the shape of a sharp cusp [60] (like in magnetic spin glasses), while we observe the Lorentzian shape according to Eq. (3) with $\gamma = 2$. It might be thought that quenched random fields smear the cusp, but some other reasons for smearing, not captured by the considered models, should also exist, as the Lorentzian shape of the small-signal $\varepsilon_s(T)$ peak was revealed both in experiment [49] and by atomic simulations [41] in the homovalent $Ba(Ti_{1-x}Zr_x)O_3$ relaxor.

Note that we do not discuss in this paper the existence in BT-DF of the true thermodynamic phase transition and the glassy freezing of dipolar dynamics in the nonergodic relaxor phase which are considered to be the features of canonical lead-oxide relaxors [2,8,32] and allowed by the soft pseudospin glass model. To obtain information about these effects using dielectric measurements, dedicated approaches are needed such as investigations of nonlinear dielectric permittivity and low-frequency dielectric dispersion. Our attempts to extract and analyze the spectrum of relaxor relaxation from the measured dielectric spectra failed, evidently because they were contaminated by a significant LFD contribution.

Let us finally discuss the difference in the behavior we observe in BT-DF, where the parameter γ characterizing the shape of the permittivity peak changes sharply at x_{F-R} and in homovalent $Ba(Ti_{1-x}Sn_x)O_3$ where $\gamma = 2$ remains unchanged around x_{F-R} [15]. This difference can be related to the increase of T_{T-O} and T_{O-R} with increasing x in the latter system which leads to the pinching effect observed at x slightly lower than x_{F-R}. The coalescence of three phase transitions

may lead to an additional broadening of the $\varepsilon(T)$ peak at $x < x_{F-R}$. In BT-DF the pinching is absent as T_{T-O} and T_{O-R} decrease rapidly with increasing x. However, the behavior is not related to random fields as T_{T-O} and T_{O-R} increase in some heterovalent systems, e.g., $BT-KNbO_3$, and decrease in some homovalent systems, e.g., $BT-SrTiO_3$ and $BT-PbTiO_3$ [61]. It was noticed [61] that any single substitution for Ba in BT always results in a lowering of T_{T-O} and T_{O-R}. When substitution is in B sites, these transition temperatures are always raised. No microscopic justification of this empirical rule has been proposed and it cannot be applied to BT-DF and other BT-based systems in which substitutions are performed in both A and B sites. We suggest that the behavior (lowing or rising) of T-O and O-R transitions in BT-based systems is determined by the variation of perovskite unit-cell volume caused by the ionic substitution. It was shown using first-principles computations that in BT the potential energy of the tetragonal ferroelectric state is slightly higher than that of the rhombohedral state, but the energy difference should decrease with decreasing unit-cell volume [57,58]. One can expect, therefore, that at small enough volume the tetragonal ground state becomes more stable than the rhombohedral one. Such volume-induced change of ground state just occurs in the BT-DF system due to the reduction of the cell volume with increasing x [Figs. 1(c) and 1(d)]. Similar microscopic arguments can be applied to justify the above-mentioned empirical rule for single A- or B-site substitutions and explain the experimentally observed effect of mixed substitutions. The radius of the Ba^{2+} cation (1.61 Å) is typically larger than the radii of isovalent cations used for single A-site substitutions (1.49, 1.44, 1.34, and 1.31 Å for Pb^{2+}, Sr^{2+}, Ca^{2+}, and Cd^{2+}, respectively), thus the substitutions lead to reduced volume and, accordingly, the transition from the rhombohedral to the tetragonal phase (through the intermediate orthorhombic phase) occurs at lower temperature. On the other hand, the radius of the Ti^{4+} cation (0.605 Å) is smaller than the radii of all cations used for single A-site substitutions (0.72, 0.69, 0.71, and 0.81 Å for Zr^{4+}, Sn^{4+}, Hf^{4+}, and Ce^{4+}, respectively), thus the low-temperature transitions rise, and the pinching occurs. Among the systems modified in both A and B sublattices, the increase of T_{O-R} is observed, for example, in $BT-LaYO_3$ [51] and $BT-KNbO_3$ [61] alongside the increase of the volume, while in $BT-DyScO_3$ both this temperature and the volume decrease [20].

V. CONCLUSIONS

The ceramics of heterovalent perovskite solid solutions $(1-x)Ba^{2+}Ti^{4+}O_3 - xDy^{3+}Fe^{3+}O_3$ are prepared in a comparatively wide concentration range of $0 \leqslant x \leqslant 0.3$, which is typically inaccessible in BT-based heterovalent systems. The T-x phase diagram of the system is constructed (Fig. 3) with the help of XRD, dielectric, and ferroelectric investigations. Three characteristic concentrations are noticed, which separate solid solutions with qualitatively different FE behavior and at which the anomalies in the dependences of some FE parameters on composition are observed.

For compositions with $x < x_{F-R} \approx 0.07$, the temperature of transition from cubic to tetragonal FE phase observed at $T_C \approx T_m$ decreases with x according to Eq. (4). The characteristic

relaxor dispersion is not observed. The shape of the $\varepsilon_s(T)$ peak at $T_m < T \leqslant T_Q$ corresponds to Eq. (3) with $1.1 < \gamma < 2$, $T_A \approx T_m$, and comparatively small δ. The Burns temperature, T_d, and the value of C are practically independent of x, while T_{CW} decreases with x, but slower than T_m.

For compositions $x_{\mathrm{F\text{-}R}} < x < x_{\mathrm{sat}} \approx 0.1$ the materials demonstrate the properties characteristic of relaxor ferroelectrics. The Burns temperature separates paraelectric and ergodic relaxor phases in these compositions. It remains practically the same as in pure BT. The transition from the cubic ergodic relaxor to the tetragonal ferroelectric phase is observed at $T_C \approx T_m$. The transition is diffuse, so that the spontaneous polarization changes slowly with temperature and reveals the "tail" at $T > T_m$ [Fig. 9(b)]. The $\varepsilon_s(T)$ peak is decreased in magnitude and can be described by Eq. (3) with $\gamma = 2$, $T_A < T_m$, and comparatively large δ. The characteristic relaxor dispersion appears, causing T_m to follow the VF law [Eq. (1)], while T_{CW} is much higher than T_m.

The compositions $x_{\mathrm{sat}} < x < x_{\mathrm{R\text{-}D}} \approx 0.2$ are also relaxors, but the phase below T_m is a macroscopically cubic nonergodic relaxor. After poling by external electric field, it transforms into the polar (ferro- or quasiferroelectric) state. The shape of the permittivity peak and the relaxor dispersion remain qualitatively the same as in the range between $x_{\mathrm{F\text{-}R}}$ and x_{sat}, but $T_m(x)$ is practically constant, T_d and T_{CW} decrease with increasing x, and T_{CW} vanishes at $x \approx x_{\mathrm{R\text{-}D}}$.

At $x > x_{\mathrm{R\text{-}D}}$, the solid solutions demonstrate the properties of normal dielectrics, rather than relaxor properties, namely, the magnitude of the permittivity peak is small, characteristic relaxor dispersion is absent, and, consequently, T_m does not depend on frequency, T_{CW} is zero, and $P(E)$ dependence is linear at all temperatures. In this composition range the shape of the permittivity peak can be fitted to Eq. (3) with $\gamma = 2$, $T_A = T_m$ both below and above T_m.

We explain the observed composition-induced evolution of ferroelectric properties by the combined effect of strong random fields related to heterovalent disorder and dilution of ferroactive Ti cations. The dilution effect contributes marginally to the decrease in Curie temperature, but it is mainly responsible for the development of relaxor properties at $x > x_{\mathrm{F\text{-}R}}$. The role of random fields is mainly to decrease T_C and the concentration of ferroelectric-to-relaxor crossover, $x_{\mathrm{F\text{-}R}}$, and to destroy the relaxor state at concentrations $x > x_{\mathrm{R\text{-}D}}$. The observed decrease in the temperatures of R-O and O-T phase transitions with increasing x is related to the decrease in the unit-cell volume.

[1] L. E. Cross, Relaxor ferroelectrics: An overview, Ferroelectrics **151**, 305 (1994).

[2] R. A. Cowley, S. N. Gvasaliya, S. G. Lushnikov, B. Roessli, and G. M. Rotaru, Relaxing with relaxors: A review of relaxor ferroelectrics, Adv. Phys. **60**, 229 (2011).

[3] Z.-G. Ye, *Handbook of Advanced Dielectric, Piezoelectric and Ferroelectric Materials: Synthesis, Properties and Applications* (Woodhead, Cambridge, 2008).

[4] E. Suna and W. Cao, Relaxor-based ferroelectric single crystals: Growth, domain engineering, characterization and applications, Prog. Mater. Sci. **65**, 124 (2014).

[5] V. V. Shvartsman and D. C. Lupascu, Lead-free relaxor ferroelectrics, J. Am. Ceram. Soc. **95**, 1 (2012).

[6] V. Westphal, W. Kleemann, and M. D. Glinchuk, Diffuse Phase Transitions and Random-Field-Induced Domain States of the "Relaxor" Ferroelectric PbMg$_{1/3}$Nb$_{2/3}$O$_3$, Phys. Rev. Lett. **68**, 847 (1992).

[7] W. Kleemann, Relaxor ferroelectrics: Cluster glass random bonds ground state via random fields and random bonds, Phys. Status Solidi B **251**, 10 (2014).

[8] A. A. Bokov and Z.-G. Ye, Recent progress in relaxor ferroelectrics with perovskite structure, J. Mater. Sci. **41**, 31 (2006).

[9] D. Phelan, C. Stock, J. A. Rodriguez-Rivera, S. Chia, J. Leão, X. Long, Y. Xie, A. A. Bokov, Z.-G. Ye, P. Ganesh, and P. M. Gehring, Role of random electric fields in relaxors, Proc. Natl. Acad. Sci. USA **111**, 1754 (2014).

[10] A. Al-Barakaty, S. Prosandeev, Dawei Wang, B. Dkhil, and L. Bellaiche, Finite-temperature properties of the relaxor PbMg$_{1/3}$Nb$_{2/3}$O$_3$ from atomistic simulations, Phys. Rev. B. **91**, 214117 (2015).

[11] A. R. Akbarzadeh, S. Prosandeev, E. J. Walter, A. Al-Barakaty, and L. Bellaiche, Finite-Temperature Properties of Ba(Zr, Ti)O$_3$ Relaxors from First Principles, Phys. Rev. Lett. **108**, 257601 (2012).

[12] W. H. Payne and V. J. Tennery, Dielectric and structural investigations of the system BaTiO$_3-$BaHfO$_3$, J. Am. Ceram. Soc. **48**, 413 (1965).

[13] S. Anwar, P. R. Sagdeo, and N. P. Lalla, Crossover from classical to relaxor ferroelectrics in BaTi$_{1-x}$Hf$_x$O$_3$ ceramics, J. Phys.: Condens. Matter **18**, 3455 (2006).

[14] N. S. Novosil'tsev and A. L. Khodakov, Dielectric properties of several solid solutions which contain barium titanate, Sov. Phys. Tech. Phys. **1**, 306 (1956).

[15] C. Lei, A. A. Bokov, and Z.-G. Ye, Ferroelectric to relaxor crossover and dielectric phase diagram in the BaTiO$_3-$BaSnO$_3$ system, J. Appl. Phys. **101**, 084105 (2007).

[16] X. Wei and X. Yao, Preparation, structure and dielectric property of barium stannate titanate ceramics, Mater. Sci. Eng. B **137**, 184 (2007).

[17] Y. Zhi, A. Chen, R. Guo, and A. S. Bhalla, Piezoelectric and strain properties of Ba(Ti$_{1-x}$Zr$_x$)O$_3$ ceramics, J. Appl. Phys. **92**, 1489 (2002).

[18] T. Maiti, R. Guo, and A. S. Bhalla, Structure-property phase diagram of BaZr$_x$Ti$_{1-x}$O$_3$ system, J. Am. Ceram. Soc. **91**, 1769 (2008).

[19] Z. Yu, C. Ang, Z. Jing, P. M. Vilarinho, and J. L. Baptista, Dielectric properties of Ba(Ti, Ce)O$_3$ from 10^2 to 10^5 Hz in the temperature range 85–700 K, J. Phys.: Condens. Matter **9**, 3081 (1997).

[20] M. C. Ferrarelli, C. C. Tan, and D. C. Sinclair, Ferroelectric, electrical, and structural properties of Dy and Sc co-doped BaTiO$_3$, J. Mater. Chem. **21**, 6292 (2011).

[21] M. Zhou, J. Zhang, L. Ji, Y. Wang, J. Wang, and F. Yu, Phase transition and piezoelectric, ferromagnetic response of B-site (Co, Nb) modified BaTiO$_3$ ceramics, Ceram. Int. **40**, 853 (2014).

[22] N. Bensemma, G. Trefalt, S. Glinšek, M. Kosec, K. Taïbi, and M. Abbaci, Investigation of the BaTiO$_3$−BaMg$_{1/3}$Nb$_{2/3}$O$_3$ system: Structural, dielectric, ferroelectric and electromechanical studies, J. Electroceram. **30**, 206 (2013).

[23] A. Munpakdee, K. Pengpat, J. Tontrakoon, and T. Tunkasiri, The study of dielectric diffuseness in the Ba(Mg$_{1/3}$Nb$_{2/3}$)O$_3$−BaTiO$_3$ ceramic system, Smart Mater. Struct. **15**, 1255 (2006).

[24] A. N. Salak, M. P. Seabra, and V. M. Ferreira, Evolution from ferroelectric to relaxor behavior in the $(1 − x)$BaTiO$_3$−xLa(Mg$_{1/2}$Ti$_{1/2}$)O$_3$ system, Ferroelectrics **318**, 185 (2005).

[25] A. Simon and J. Ravez, New lead-free perovskite relaxor ceramics derived from BaTiO$_3$ and containing scandium, J. Adv. Dielectrics **1**, 251 (2011).

[26] R. L. White, Review of recent work on the magnetic and spectroscopic properties of the rare-earth orthoferrites, J. Appl. Phys. **40**, 1061 (1969).

[27] Y. Tokunaga, S. Iguchi, T. Arima, and Y. Tokura, Magnetic-Field-Induced Ferroelectric State in DyFeO$_3$, Phys. Rev. Lett. **101**, 097205 (2008).

[28] T. Nakajima, Y. Tokunaga, Y. Taguchi, Y. Tokura, and T. Arima, Piezomagnetoelectric Effect of Spin Origin in Dysprosium Orthoferrite, Phys. Rev. Lett. **115**, 197205 (2015).

[29] J. Zhuang, L.-W. Su, H. Wu, A. A. Bokov, M. Liu, W. Ren, and Z.-G. Ye, Coexisting ferroelectric and magnetic morphotropic phase boundaries in Dy-modified BiFeO$_3$−PbTiO$_3$ multiferroics, Appl. Phys. Lett. **107**, 182906 (2015).

[30] J. Zhuang, L.-W. Su, J. Zhao, H. Wu, A. A. Bokov, W. Ren, and Z.-G. Ye, Structure and local polar domains of Dy-modified BiFeO$_3$−PbTiO$_3$ multiferroic solid solutions, J. Mater. Chem. C **3**, 12450 (2015).

[31] A. A. Coelho, A bound constrained conjugate gradient solution method as applied to crystallographic refinement problems, J. Appl. Cryst. **38**, 455 (2005).

[32] A. A. Bokov and Z.-G. Ye, Dielectric relaxation in relaxor ferroelectrics, J. Adv. Dielectrics **2**, 1241010 (2012).

[33] A. K. Jonscher, *Universal Relaxation Law* (Chelsea Dielectric, London, 1996).

[34] V. V. Lemanov, Barium titanate-based solid solutions, Ferroelectrics **354**, 69 (2007).

[35] V. L. Gurevich and A. K. Tagantsev, Intrinsic dielectric loss in crystals, Adv. Phys. **40**, 719 (1991).

[36] D. Viehland, S. J. Jang, L. E. Cross, and M. Wuttig, Freezing of the polarization fluctuations in lead magnesium niobate relaxors, J. Appl. Phys. **68**, 2916 (1990).

[37] D. Nuzhnyy, J. Petzelt, M. Savinov, T. Ostapchuk, V. Bovtun, M. Kempa, J. Hlinka, V. Buscaglia, M. T. Buscaglia, and P. Nanni, Broadband dielectric response of Ba(Zr, Ti)O$_3$

[38] ceramics: From incipient via relaxor and diffuse up to classical ferroelectric behavior, Phys. Rev. B **86**, 014106 (2012).

[38] G. Rupprecht and R. O. Bell, Dielectric constant in paraelectric perovskites, Phys. Rev. **135**, A748 (1964).

[39] H. Yu and Z.-G. Ye, Dielectric properties and relaxor behavior of a new $(1 − x)$BaTiO$_3$−xBiAlO$_3$ solid solution, J. Appl. Phys. **103**, 034114 (2008).

[40] A. K. Jonscher, *Dielectric Relaxation in Solids* (Chelsea Dielectric, London, 1983).

[41] D. Wang, J. Hlinka, A. A. Bokov, Z.-G. Ye, P. Ondrejkovic, J. Petzelt, and L. Bellaiche, Fano resonance and dipolar relaxation in lead-free relaxors, Nat. Commun. **5**, 5100 (2014).

[42] D. Wang, A. A. Bokov, Z.-G. Ye, J. Hlinka, and L. Bellaiche, Subterahertz dielectric relaxation in lead-free Ba(Zr, Ti)O$_3$ relaxor ferroelectrics, Nat. Commun. **7**, 11014 (2016).

[43] V. V. Kirilov and V. A. Isupov, Relaxation polarization of PbMg$_{1/3}$Nb$_{2/3}$O$_3$(PMN): A ferroelectric with a diffused phase transition, Ferroelectrics **5**, 3 (1973).

[44] R. Clarke and J. C. Burfoot, The diffuse phase transition in potassium strontium niobate, Ferroelectrics **8**, 505 (1974).

[45] I. A. Santos and J. A. Eiras, Phenomenological description of the diffuse phase transition in ferroelectrics, J. Phys.: Condens. Matter **13**, 11733 (2001).

[46] A. A. Bokov, Y.-H. Bing, W. Chen, Z.-G. Ye, S. A. Bogatina, I. P. Raevski, S. I. Raevskaya, and E. V. Sahkar, Empirical scaling of the dielectric permittivity peak in relaxor ferroelectrics, Phys. Rev. B **68**, 052102 (2003).

[47] C. Lei, A. A. Bokov, and Z.-G. Ye, Relaxor behavior in Ba(Ti$_{0.72}$Sn$_{0.28}$)O$_3$ solid solution, Ferroelectrics **339**, 129 (2006).

[48] W.-M. Zhu, H.-Y. Guo, and Z.-G. Ye, Structural and magnetic characterization of multiferroic $(1 − x)$BiFeO$_3$−xPbTiO$_3$ solid solutions, Phys. Rev. B **78**, 014401 (2008).

[49] A. A Bokov, M. Maglione, and Z.-G. Ye, Quasi-ferroelectric state in Ba(Ti$_{1−x}$Zr$_x$)O$_3$ relaxor: Dielectric spectroscopy evidence, J. Phys.: Condens. Matter **19**, 092001 (2007).

[50] M. Fukunaga, G. Li, Y. Uesu, and K. Kohn, Structural and dielectric properties of nickel-doped and lanthanum-chromium-doped barium titanate ceramics, Jpn. J. Appl. Phys. **41**, 6926 (2002).

[51] A. Feteira, D. C. Sinclair, and M. T. Lanagan, Effects of average and local structure on the dielectric behavior of $(1 − x)$BaTiO$_3$−xLaYO$_3$ $(0 \leqslant x \leqslant 0.40)$ ceramics, J. Appl. Phys. **108**, 014112 (2010).

[52] J. R. Arce-Gamboa and G. G. Guzmán-Verri, Random electric field instabilities of relaxor ferroelectrics, npj Quantum Mater. **2**, 28 (2017).

[53] J. Li, D. Zhang, S. Qin, T. Li, M. Wu, D. Wang, Y. Bai, and X. Lou, Large room-temperature electrocaloric effect in lead-free BaHf$_x$Ti$_{1−x}$O$_3$ ceramics under low electric field, Acta Mater. **115**, 58 (2016).

[54] C. Laulhé, A. Pasturel, F. Hippert, and J. Kreisel, Random local strain effects in homovalent-substituted relaxor ferroelectrics: A first-principles study of BaTi$_{0.74}$Zr$_{0.26}$O$_3$, Phys. Rev. B **82**, 132102 (2010).

[55] Y. Imry and S.-k. Ma, Random-Field Instability of the Ordered State of Continuous Symmetry, Phys. Rev. Lett. **35**, 1399 (1975).

[56] D. Sherrington, BZT: A Soft Pseudospin Glass, Phys. Rev. Lett. **111**, 227601 (2013).

[57] R. E. Cohen and H. Krakauer, Lattice dynamics and origin of ferroelectricity in BaTiO$_3$: Linearized-augmented-plane-wave total-energy calculations, Phys. Rev. B **42**, 6416 (1990).

[58] R. E. Cohen, Origin of ferroelectricity in perovskite oxides, Nature (London) **358**, 136 (1992).

[59] N. A. Hill, Why are there so few magnetic ferroelectrics? J. Phys. Chem. B **104**, 6694 (2000).

[60] D. Sherrington, A spin glass perspective on ferroic glasses, Phys. Status Solidi B **251**, 1967 (2014).

[61] R. J. Bratton and T. Y. Tien, Phase transitions in the system BaTiO$_3$−KNbO$_3$, J. Am. Ceram. Soc. **50**, 90 (1967).